Ground Motion Prediction Equations Derived from the Italian Strong Motion Database

Bindi D. (1)*, Pacor F.(2), Luzi L.(2), Puglia R. (2), Massa M. (2), G. Ameri (2) and R. Paolucci (3)

(1) Deutsches GeoForschungsZentrum GFZ, Centre for Disaster Managment (CEDIM), Telegrafenberg, 14473 Potsdam, Germany
(2) Istituto Nazionale di Geofisica e Vulcanologia, Sezione Milano-Pavia, via Bassini 15, 20133 Milano, Italy
(3) Politecnico di Milano, Dipartimento di Ingegneria Strutturale, Piazza Leonardo da Vinci, 32 20133 Milano, Italy

*on leave from Istituto Nazionale di Geofisica e Vulcanologia, Sezione Milano-Pavia

Abstract

We present a set of ground motion prediction equations (GMPEs) derived for the geometrical mean of the horizontal components and the vertical, considering the latest release of the strong motion database for Italy. The regressions are performed over the magnitude range 4 - 6.9 and considering distances up to 200 km. The equations are derived for peak ground acceleration (PGA), peak ground velocity (PGV) and 5%-damped spectral acceleration at periods between 0.04 and 2 s. The total standard deviation (sigma) varies between 0.34 and 0.38 $\log_{10}$ unit, confirming the large variability of ground shaking parameters when regional data sets containing small to moderate magnitude events ($M < 6$) are used. The between-stations variability provides the largest values for periods shorter than 0.2 s while, for longer periods, the between-events and between-stations distributions of error provide similar contribution to the total variability.

Introduction

This special issue of the Bulletin of Earthquake Engineering collects several studies carried out in the framework of the project "S4 - Italian strong motion database" (Pacor et al., 2011), funded by the Italian Department of Civil Protection (DPC), in order to improve the quality of the Italian strong motion database ITACA (Luzi et al., 2008; Pacor et al.; 2011; http://itaca.mi.ingv.it). In this paper, we exploit such improvements to update the ground motion prediction equation (GMPE) developed for Italy by Bindi et al (2010), hereinafter referred to as ITA08. Several reasons motivated this update. Besides the enrichment of the database with the recordings relevant to the 2009 L'Aquila seismic sequence, whose mainshock (Mw = 6.3) provided data over a magnitude - distance range scarcely sampled in ITACA, a re-processing of the whole data set has performed within the project S4 (Paolucci et al., 2011), in order to obtain compatible acceleration, velocity and displacement time series. Furthermore, in the framework of the same project, several field surveys were carried out to improve the geophysical characterization of the recording sites (Foti et al., 2011), significantly increasing the number of measured shear-wave profiles, used here to classify the sites accordingly to the Eurocode8 (CEN, 2003). Finally, to improve the usability of the model, the distance range is extended from 100 to 200 km and the style of faulting has been included among the explanatory variables.

This article is organized as follows. First, the data-set used to derive the new GMPEs is described and compared to data-set used to develop the ITA08 model. Then, the results of new regressions are presented both in terms of average models and associated variability. Finally, the comparison with ITA08 is shown.

Data Set

From the whole ITACA database a first selection is performed by considering only magnitudes larger than 4, epicentral distances smaller than 200 km and hypocentral depths shallower than 35 km. By applying these criteria, 1213 recordings from 218 earthquakes and 353 stations are selected. The magnitude versus distance scatter plot is shown in Figure 1. It is worth noting that the local magnitude (Ml, magenta symbols in Figure 1) is the only magnitude estimate available for most of the events with magnitude

smaller than 4.5, as quantified by the histogram in the right panel. Moreover, a significant number of stations recorded only one earthquake. A further selection is performed by removing the earthquakes missing the estimate of the moment magnitude, those recorded by one station and the stations with one record only. Overall, 769 records relevant to 99 earthquakes and 150 stations are selected to update the GMPEs for Italy over the magnitude range $4.1 \leq Mw \leq 6.9$. Hereinafter we refer to the updated model as ITA10.

The focal mechanisms of the events extracted from ITACA are categorized into four classes (Normal: 593 records; Reverse:87; Strike Slip:61; Unknown: 28), following the classification by Zoback (1992), as described in Luzi et al. (2008). The focal mechanism distribution of the dataset is shown in Figure 2.

Most of events were caused by normal faults in central and southern Apennines, such as the 1980, M 6.9, Irpinia earthquake; the 1997, M 6.0, Umbria-Marche earthquake; the 2009, M 6.3, L'Aquila earthquake. The focal depths for the normal earthquakes is generally shallower than 20 km. Compressional tectonic regime is peculiar to earthquakes occurred in the North-Eastern Italy (eg. the Mw = 6.4, 1976 Friuli earthquake) and in the Northern Apennines. The focal depth of these earthquakes is generally deeper than 15 km. Finally, strike-slip events (e.g., the Mw 5.7, 2002 Molise earthquake) mainly occurred in southern Italy at focal depths between 10 and 30 km.

The comparison between ITA08 and this study, in terms of magnitude distributions, is shown in Figure 3 (Left). The total number of records increases from 561 to 769. In particular, the records of the L'Aquila sequence increased the number of accelerograms for magnitudes between 4.5 and 6.

In Figure 3 (right), the magnitude versus distance distribution of the ITA10 and the ITA08 data sets is shown. Most of the records included in ITA08 and discarded in this study (green circles) are from small magnitude earthquakes or correspond to stations with one record.

Distances larger than 10km are well sampled over the entire magnitude range, while the records for distances shorter than 5 km are mainly from earthquakes with $M \leq 6$. The number of near-fault recordings has been increased in ITA10 by adding 5 recordings with Joyner-Boore distance Rjb = 0 km from the M 6.3, L'Aquila earthquake, and 6 records

from the 1976-77 Friuli seismic sequence recorded by the analog station installed at Gemona (GMN) and characterized by Rjb distances shorter than 6 km.

In ITA08 a simplified scheme was adopted to classify sites, based on Sabetta and Pugliese (1986). Three classes were considered: "rock" (class 0, rock outcrops or deposits with thickness lower than 5m), "shallow alluvium" (class 1, deposits with thickness lower than or equal to 20m) and "deep alluvium" (class 2 deposits with thickness greater than 20m), where alluvium refers to deposits with shear wave velocity between 400 m/s and 800 m/s. The three classes are well sampled by the ITA08 dataset (Figure 4, Left).

Conversely, in this study the recording sites are classified into 5 classes, based on the shear wave velocity intervals in the uppermost 30 m, Vs_{30}, according to the EC8 (CEN, 2003): class A: $Vs_{30} > 800$ m/s; class B: Vs_{30}=360 - 800 m/s; class C: Vs_{30} = 180 - 360 m/s; class D: $Vs_{30} < 180$ m/s; class E: 5 to 20 m of C- or D-type alluvium underlain by stiffer material with $Vs_{30} > 800$ m/s. The Vs_{30} values were obtained either from measurements (about 30%) or inferred by geological and geophysical data. This classification was feasible thanks to the improvements of the geological, geotechnical and geophysical information contained in the new release of the ITACA database. Classes D and E are poorly sampled with 18 and 37 records, respectively, while the other classes are well represented with 247, 199 and 180 records (Figure 4, right panel)

The two data sets share 108 stations (Figure 5). As expected, most rock sites (class 0) and deep alluvium (class 1) of ITA08 correspond to classes A and B-C of ITA10, respectively. Conversely, the shallow alluvium sites (class 1, ITA08) are re-distributed among all the EC8 classes except class D.

Finally, we recall that the following procedure has been applied to process the ITA10 data (Paolucci et al., 2011): 1) baseline correction; 2) application of a cosine taper, based on the visual inspection of the record (typically between 2% and 5% of the total record length); records identified as late-triggered are not tapered; 3) visual inspection of the Fourier spectrum to select the band-pass frequency range; 4) application of a 2nd order a-causal time-domain Butterworth filter to the acceleration time-series padded with zeros; 5) double-integration to obtain displacement time series; 6) linear de-trending of displacement and 7) double-differentiation to get the corrected acceleration. The applied procedure is similar to the one adopted to process the ITA08 data set, except for steps 5-7

which ensures the compatibility among acceleration, velocity and displacement time series and a particular attention was paid to the treatment of late triggered records (see Paolucci et al., 2011 for details).

Functional form

The equation used for the regression is similar to the model adopted by Boore and Atkinson (2008), although a different site classification is used and the non-linear site terms neglected. The functional form is the following:

$$\log_{10} Y = e_1 + F_D(R, M) + F_M(M) + F_S + F_{sof} \quad (1)$$

where e_1 is the constant term, $F_D(R, M)$, $F_M(M)$, F_s and F_{sof} represent the distance function, the magnitude scaling, the site amplification and the style of faulting correction, respectively. M is the moment magnitude, R is the Joyner-Boore distance, or the epicentral distance (in km), when the fault geometry is unknown (generally when M < 5.5).

The strong motion parameters Y considered for the regressions are the peak ground acceleration (PGA, in cm/s^2) and velocity (PGV, cm/s) and the 5%-damped absolute acceleration response spectra (Sa, cm/s^2) in the period range 0.04 to 2s. The proposed equation for the distance function is:

$$F_D(R, M) = \left[c_1 + c_2\left(M - M_{ref}\right)\right]\log_{10}\left(\sqrt{R_{JB}^2 + h^2} / R_{ref}\right) - c_3\left(\sqrt{R_{JB}^2 + h^2} - R_{ref}\right) \quad (2)$$

while the magnitude function is:

$$F_M(M) = \begin{cases} b_1\left(M - M_h\right) + b_2\left(M - M_h\right)^2 & \text{for } M \le M_h \\ b_3\left(M - M_h\right) & \text{otherwise} \end{cases} \quad (3)$$

where M_{ref}, M_h, R_{ref} are coefficients to be determined through the analysis. Differently from the model used to develop ITA08, $F_D(R,M)$ now includes a term linearly decreasing with distance (anelastic attenuation) and $F_M(M)$ considers the hinge magnitude M_h.

The functional form F_S in equation (1) represents the site amplification and it is given by $F_S = s_j C_j$, for j=1,...5, where s_j are the coefficients to be determined through the regression analysis, while C_j are dummy variables used to denote the five different EC8 site classes (A_{EC8} through E_{EC8}). The functional form F_{sof} represents the style of faulting correction and it is given by $F_{sof} = f_j E_j$, for j=1,...4, where f_j are the coefficients to be determined during the analysis and E_j are dummy variables used to denote the different fault classes. We considered 4 types of style of faulting: normal (N), reverse (R), strike slip (SS) and unknown (U). The distributions of the analyzed recordings for different style of faulting and site classes are shown in Figure 2 and Figure 4. It is worth noting that class U could be dominated by earthquakes belonging to a particular class (e.g. normal).

After some trial regressions and after Boore and Atkinson (2008), the following variables have been fixed: $R_{ref} = 1$ km; $M_{ref} = 5$; $M_h = 6.75$; $b_3 = 0$. The regressions are performed by applying a random effect approach (Abrahamson and Youngs, 1992). In agreement with the GMPEs recently developed for Europe (Akkar and Bommer, 2010) and Turkey (Akkar et al., 2010), the regressions are developed considering the geometrical mean of the as-recorded horizontal components (hereinafter GeoH), while ITA08 was derived considering the maximum between the horizontal components. Furthermore, the regressions for the vertical component (hereinafter Z) are performed as well. Each regression is performed twice: in the first one, the between-events and within-event components of variability are separated while in the second one the between- and within-station components are determined (e.g., Bindi et al 2006; Bindi et al., 2009). For the definition of the components of variability, see Al Atik et al. (2010).

Determination of the coefficients

The regression coefficients and standard deviations obtained for GeoH and Z are shown in Tables from 1 to 6. For each period the standard deviation of the distribution of the coefficients is obtained through a bootstrap analysis (Efron and Tibshirani, 1994)

considering 40 different bootstrap replications of the original data set. Each replication is randomly selected and composed by the same number of data as the original data set.

The existence of trade-offs among different parameters can be detected by analyzing the off-diagonal elements of the unit covariance matrix (Menke, 1989), shown in Figure 6, for Sa at 0.1 s (top) and 1s (bottom). The design matrix used to compute the covariance matrix is the Jacobian matrix derived from equation (1) and evaluated considering the final value of the regression coefficients. The covariance matrix shows that a trade off between the off-set coefficient e_1 and several others parameters exists. Examples, for Sa at 0.1 s, are: the negative trade-off with c_1 ($C_{1,2}$=-1.621) and c_2 ($C_{1,3}$=-0.061) and positive trade-off with b_1 ($C_{1,6}$= 0.281). The pseudo-depth parameter h shows a strong positive trade-off with e_1 ($C_{1,4}$=0.278) and a strong negative trade-off with c_1 ($C_{2,4}$=-0.267), probably as a consequence of the scarce sampling of distances shorter than 10km. The diagonal elements of the unit covariance matrix represent the amplification factors for the propagation of error from data to the solution. Figure 6 shows that the largest amplifications affect the variance of the coefficients e_1 ($C_{1,1}$=0.580 at 0.1 s), b_1 ($C_{2,2}$=0.128 at 0.1 s) and h ($C_{4,4}$=2.125 at 0.1 s), with decreasing amplitude for increasing period ($C_{1,1}$=0.267, $C_{2,2}$=0.057 and $C_{4,4}$=2.0 at 1 s). The site coefficients more affected by the propagation of error are s_4 ($C_{10,10}$=0.064 at 0.1 s) and s_5 ($C_{11,11}$= 0.031 at 1s), corresponding to the site classes less sampled by data.

Figure 7 shows the obtained site (s_2, s_3, s_4, s_5) and style of faulting (f_N, f_{SS}, f_R) coefficients for both GeoH and Z models.

The regressions were developed constraining the coefficient s_1 (class A_{EC8}) to zero. For the horizontal components, s_2 (class B_{EC8}) is almost constant and equal to 0.2, while the coefficient s_3 (class C_{EC8}) is about 0.25 at T = 0.1s and increases to 0.33 at 2 s. The coefficients for class D and E exhibit a large peak at about 1 and 0.15 s, respectively. The results for class D and E should be considered taking into account the small number of stations populating the two classes. In particular, 33 out of 37 available recordings for class E are relevant to the co-located instruments (NCR, analog) and (NCR2, digital), installed at the Nocera Umbra (Central Italy) station. The site response of Nocera Umbra station has been deeply investigated by previous studies demonstrating that large amplifications occur around 6 Hz (e.g., Rovelli et al., 2002; Castro et al., 2004; Luzi et al,

2005). For this reasons the amplitude of coefficient s_5 as a function of period, shown in Figure 7, mostly represents the site effect of station NCR/NCR2. Similarly, 16 out of 19 recordings available for class D are relative to two stations in central Italy: CLF, installed in Colfiorito (12 records), and NOR, installed in Norcia (5 recordings). Both stations show a clear site amplification around 1 Hz (Rovelli et al., 2001; Bindi et al., 2009), as for coefficient s_4. As a consequence, the coefficients s_4 and s_5 mainly represent a correction for the site amplification affecting the recordings of stations CLF and NCR/NCR2, respectively.

In order to assess the effect of including classes D and E on the median model, the regression was also performed removing the records relative to these two classes. A difference smaller than 10% in the median predictions (here not shown) was observed at 1s at distances smaller than 10 km but, in general, we can conclude that the presence of data from classes D and E in the regression has a small effect in the bias of the median predictions for the other classes, as expected from the analysis of the covariance matrixes.

When the vertical component is considered, it can be observed that coefficients similar to the horizontal components are obtained for classes B and C (Figure 7). For class D and E, the site coefficients for the vertical components show amplifications over the long and short period range, respectively, but with smaller amplitude with respect to the horizontal component. Moreover, the peak observed for class D is shifted towards shorter periods (0.7 s) with respect to GeoH (1 s).

Figure 7 also shows the style of faulting coefficients obtained for GeoF and Z. We constrained to zero the style of faulting coefficient f_4 (the unknown class). The average of the style of faulting coefficients was also constrained to zero ($f_1 + f_2 + f_3 = 0$), in order to include in the offset coefficient e_1 (equation 1) the average effect of the faulting mechanism. For short periods ($T < 0.1$s) and horizontal components, f_2 (reverse mechanism) is positive (about 0.08) while both f_1 (normal) and f_3 (strike slip) are negative (about -0.03). The coefficient f_3 tends to be slightly larger than f_2 in the period range $0.2 < T < 0.7$s and the trend inverts f_3 for longer periods ($T > 1$s). These trends confirm that the main differences in the ground motion for different focal mechanisms are observable over the medium-to-short period range ($T < 1$s), where the predictions for reverse

mechanism are visibly larger than those for the other styles of faulting. For the vertical components the differences between strike-slip and normal mechanisms are more evident than the horizontal component over the medium-to-short period range (T < 1s).

Several tests (not shown here) were performed assuming different constraints for the style of faulting coefficients. In particular, the following cases were considered: 1) coefficient of normal earthquakes constrained to zero; 2) coefficient of unknown focal mechanisms constrained to zero; 3) average of the four style of faulting coefficients constrained to zero. The results show that the constraints applied to the style of faulting coefficients does not affect the median predictions, but only the values of the coefficients themselves.

Finally, a comparison between records and median predictions of the model derived in this study was made for different magnitudes and styles of faulting (Figure 8). The PGA and PGV predicted for B_{EC8} are compared to the observations of different EC8 soil classes for three significant earthquakes occurred in Italy characterized by different fault mechanisms (i.e., the M_w = 6.9, 1980 Irpinia earthquake; the M_w = 5.7, 2002 Molise earthquake; the M_w = 6.4, 1976 Friuli earthquake). The comparison for a magnitude 4.6 and unknown style of faulting is performed as well, with the observations from 5 earthquakes. A general good agreement is observed for all earthquakes, independently of magnitude and focal mechanism.

Analysis of residuals

Figure 9 (left) shows the total standard deviation (σ_{tot}) as function of period, as well as the between-events and within-event components. The total standard deviation varies from 0.34 to 0.38 (in $\log_{10}$ units) with the largest contribution coming from the within-event variability. In particular, if the random effect model is applied to estimate the between-stations variability (right panel), we observe that, for periods shorter than about 0.2 s, the between-stations component is larger than the between-events one, while for periods longer than 0.4 sec, the two components of variability are similar.

Figure 9 also reports the σ_{tot} of ITA08. The standard deviations for the two models are similar, with a slight reduction obtained in this study for periods longer than 0.3 s. For both models, the variability over the short period range (<0.4 s) is dominated by the between stations variability, which is very similar (right panel). For periods longer than

0.4 s, a reduction of the between stations variability is obtained in this study with respect to ITA08. This result suggests that the EC8 classification improves the long-period seismic response of soft and very soft sites, but it might not be suitable to capture the large high frequency variability of the response for the Italian sites.

Figure 10 shows the within-event (i.e. the residual corrected for the between events term) distribution of error as function of the distance from the source and the between-events residuals versus magnitude. Both distributions confirm that the derived model produces unbiased estimates of the observations, with residuals independent on the explanatory variables (i.e. magnitude and distance).

Comparison with ITA08

In Figure 11 the predictions for an earthquake with $M_w = 6.3$ are compared to the strong motion data of the 2009 L'Aquila earthquake, considering PGA and the spectral acceleration at 1s and three soil classes (EC8 A through C, from top to bottom, respectively). The predictions from the GMPE developed in this study and from ITA08 are also compared. L'Aquila mainshock has been densely recorded by the national strong motion network (Ameri et al., 2009) and data from 49 stations in the distance range 0<=Rjb<=200 km are available in the ITACA database. In addition, down-hole, cross-hole and SASW tests have been performed at the near source stations, in order to characterize the sites that constrain the attenuation at short distances. On average, the predictions match reasonably well the observations over the entire distance range, for both periods. In particular, a good agreement is observed between the predicted acceleration level at $R_{JB} = 0$ and recorded data for class B_{EC8}. Since ITA08 was derived considering the maximum horizontal component at each period, we applied the correction coefficients proposed by Beyer and Bommer (2006). Moreover, we used the site coefficients for classes 0, 1, and 2 to perform the comparison with classes A, B, and C of EC8, respectively. In general, the median predictions of ITA08 are lower than this study at distances smaller than 10 km for Sa at 1 s, and they show weaker attenuation with distance, especially for PGA. For lower magnitudes (i.e. 4.6, as shown in Figure 12) and short to intermediate periods (PGA and Sa at 1s) the median prediction and the error associated are similar, as the ITA08 and the ITA10 data sets do not differ substantially.

For the vertical component, the main differences for PGA are observed at short distances for class C, where the ground motion predicted by ITA10 is stronger than ITA08 (Figure 13, right panels). When compared to ITA08, the vertical PGA predicted by ITA10 attenuates faster with distance for all the considered soil classes. A better agreement between the ITA10 and ITA08 predictions is observed for spectral acceleration at 1 s (left panels), especially for classes A and C.

Conclusions

We developed a set of GMPEs for Italy using the recently compiled strong motion database (ITACA, http://itaca.mi.ingv.it). The regressions have been performed for PGA, PGV and spectral acceleration, considering the geometrical mean of the NS and EW components, and the vertical component, over the magnitude range 4 - 6.9 and for distances up to 200 km. The model is well calibrated, matching the observation without any significant bias affecting the between-events or the within-event distribution of errors. The total standard deviation (σ_{tot}) varies between 0.34 and 0.38 $\log_{10}$ unit, confirming the large variability of ground shaking parameters when regional data sets containing small to moderate magnitude events ($M < 6$) are explored (Douglas, 2007), as also observed for the GMPE derived for Turkey (Akkar and Cagnan, 2011, their Figure 6).

The between-stations and the between-events contributions to the total variability appear to be the most important, with a dominance of the between-events sigma at periods longer than 0.3s and of the between-stations sigma over the short period range.

This set of new GMPEs improves the existing attenuation equation recently derived for Italy (ITA08, Bindi et al., 2010) and it is recommended for many reasons:

1) the data set is enlarged and the magnitude distance sampling improved. In particular, relevant data have been introduced to constrain the near source ground motion, recorded during the recent 2009 M_w 6.3 l'Aquila earthquake;
2) the range of distance has been extended to 200 km, introducing the anelastic term in the distance function;
3) the style-of-faulting coefficients are considered;
4) EC8 (CEN, 2003) site classification has been adopted.

Relevant results with this work are obtained in predicting moderate magnitude-events in the near fault, after the introduction of the L'Aquila mainshock records. The expected ground motion increases significantly (two or three times) in the vicinity of the fault for all soils classes and intermediate to long periods.

The extension in the considered distance range and the introduction of the anelastic attenuation term results in a faster attenuation of the high frequency motion (i.e. PGA) after 30 km both for the horizontal and vertical components. Furthermore the introduction of a soil classification based on the shear wave velocity of the uppermost 30 m allows different applications of this GMPE, such as Shake map calculation and comparison with the spectral shapes of Eurocode 8 and the Italian seismic code.

Acknowledgments

Constructive comments from two reviewers (J. Bommer and Z. Cagnan) are strongly acknowledged. The strong ground motion data used in the present article can be down-loaded from the ITACA database: http://itaca.mi.ingv.it. All the information about the database are included in the Deliverables of the project "Italian Strong motion database" funded by the Italian Department of Civil Protection (DPC), in the framework of the agreement 2005-2007 with the Italian Institute of Geophysics and Vulcanology (INGV). The figures in this work have been drawn with the Generic Mapping Tool (GMT) software (Wessel and Smith, 1991). The excel table containing the coefficients is available on request to the corresponding author.

References

Abrahamson, N. A., and R. R. Youngs (1992). A stable algorithm for regression analyses using the random effects model, Bull. Seismol. Soc. Am. 82, 505–510

Akkar, S. and J.J. Bommer (2010). Empirical equations for the prediction of PGA, PGV and spectral accelerations in Europe, the Mediterranean region and the Middle East, Seismological Research Letters, 81, 195-206.

Akkar, S., Z. Çagnan, E. Yenier, Ö. Erdoğan, A. Sandıkkaya and P. Gülkan (2010). The recently compiled Turkish strong motion database: preliminary investigation for seismological parameters, Journal of Seismology,14, 457-479

Akkar, S., and Z. Cagnan, (2010). A local ground-motion predictive model for Turkey and its comparison with other regional and global ground-motion models, Bulletin of the Seismological Society of America, 100, 2978-2995

Al Atik, L., N. Abrahamson, J.J. Bommer, F. Scherbaum, F. Cotton, and N. Kuehn (2010). The Variability of Ground-Motion Prediction Models and Its Components, Seismological Research Letters, 81,. 794-801; DOI: 10.1785/gssrl.81.5.794

Ameri, G., M. Massa, D. Bindi, E. D'Alema, A. Gorini, L. Luzi, S. Marzorati, F. Pacor, R. Paolucci, R. Puglia, and C. Smerzini (2009). The 6 April 2009 Mw 6.3 L'Aquila (Central Italy) Earthquake: Strong-motion Observations, Seism Res Lett, 80: 951 - 966. doi: 10.1785/gssrl.80.6.951

Beyer, K., and JJ. Bommer (2006). Relationships between median values and between aleatory variabilities for different definitions of the horizontal component of motion, Bulletin of the Seismological Society of America, 96, 1512-1522.

Bindi D, Luzi L, Pacor F, Franceschina G, and R. R. Castro (2006) Ground-Motion prediction from empirical attenuation relationships versus recorded data: the case of the 1997–1998 Umbria-Marches, Central Italy, Strong Motion Data Set, Bull Seismol Soc Am 96(3):984–1002. doi:10.1785/0120050102

Bindi D, Luzi L, and F. Pacor (2009). Interevent and Interstation Variability Computed for the Italian Accelerometric Archive (ITACA) Bull Seismol Soc Am; 99(4): 2471-2488. doi: 10.1785/0120080209

Bindi, D., L. Luzi, M. Massa, and F. Pacor (2010). Horizontal and vertical ground motion prediction equations derived from the Italian Accelerometric Archive (ITACA), Bull Earthquake Eng (2010) 8:1209–1230, doi 10.1007/s10518-009-9130-9

Boore, D.M. and G.M. Atkinson (2008). Ground-Motion Prediction Equations for the Average Horizontal Component of PGA, PGV, and 5%-Damped PSA at Spectral Periods between 0.01s and 10.0s, Earthquake Spectra, 24, 99-138.

Castro, R.R., Pacor, F., Bindi D., Franceschina G., and L. Luzi (2004). Site Response of Strong Motion Stations in the Umbria Region, Central Italy, Bull. Seismol Soc. Am. 94, 576–590.

CEN (Comité Européen de Normalisation) (2003). prEN 1998-1- Eurocode 8: Design of structures for earthquake resistance. Part 1: General rules, seismic actions and rules for buildings. Draft No 6, Doc CEN/TC250/SC8/N335, January 2003, Brussels.

Douglas, J. (2007). On the regional dependence of earthquake response spectra: ISET Journal of Earthquake Technology, 44, 1, , p. 471–499.

Efron, B., and R. J. Tibshirani (1994). An Introduction to the Bootstrap, Chapman & Hall/CRC, Boca Raton, Florida, ISBN 978-0412042317, 456 pp.

Foti S., Parolai S., Bergamo P., Di Giulio G., Maraschini M., Milana G., Picozzi M., Puglia R. (2011). Surface wave surveys for seismic site characterization of accelerometric stations in ITACA, Bulletin of Earthquake Engineering, this issue

Luzi, L., D. Bindi, G. Franceschina, F. Pacor, and R. R. Castro (2005). Geotechnical Site Characterisation in the Umbria Marche Area and Evaluation of Earthquake Site-Response. Pure Appl. Geoph. 162, 2133–2161.

Luzi L., Sabetta F., Hailemikael S., Bindi D., Pacor F., and F. Mele (2008). ITACA (ITalian ACcelerometric Archive): a web portal for the dissemination of Italian strong motion data. Seism Res Lett 79(5): 717–723. doi:10. 1785/gssrl.79.5

Menke, W. (1989). Geophysical data analysis: discrete inverse theory, in Int. Geophys. Series, R. Dmowska and J. R. Holton (Series Editors), Vol. 45, Academic Press, New York, 289 pp.

Pacor F., Paolucci R. , Luzi L., Sabetta S., Dolce M., , Gorini A. , De Sortis A. and A. Spinelli (2011). Overview of the Italian strong motion database 1.0. Submitted to Bull Earth. Eng, this Special Issue.

Paolucci R., Pacor F., Puglia R., Ameri G., Cauzzi C. and M. Massa (2011). Record processing in ITACA, the new Italian strong-motion database. In Earthquake Data in Engineering Seismology. Predictive Models, Data Management and Networks, *Eds S. Akkar, P. Gulkan and T. Van Eck,* Geotechnical, Geological and Earthquake Engineering series, Vol. 14, Chapter 8, 99-113, Springer.

Rovelli, A., A. Caserta, F. Marra, and V. Ruggiero (2002). Can seismic waves be trapped inside an inactive fault zone? The case study of Nocera Umbra, central Italy, Bull. Seismol. Soc. Am. 92, 2217–2232.

Rovelli, A., L. Scognamiglio, F. Marra, and A. Caserta (2001). Edge diffracted 1-sec surface waves observed in a small-size intramountain basin (Colfiorito, central Italy), Bull. Seismol. Soc. Am. 91, 1851–1866.

Sabetta F, and A. Pugliese (1996) Estimation of response spectra and simulation of non-stationary earthquake ground motions. Bull Seismol Soc Am 86(2):337–352

Wessel, P., and W. H. F. Smith (1991). Free software helps map and display data, Eos Trans. AGU 72, no. 41, 445–446.

Zoback, M. L. (1992). First- and second-order patterns of stress in the lithosphere: The World Stress Map Project. Journal of Geophysical Research 97 (B8), 11,703–11,728.

Figure Captions

Figure 1 - ITACA dataset from events with M > 4. Left: magnitude versus distance scatter plot. Right: histogram of the records grouped according to earthquake magnitude. . Grey symbols represent the records used to calibrate the ITA10 GMPEs. Magenta symbols represent records lacking of the moment-magnitude. Green symbols represent the records from events recorded by one station or from stations with one record. The coloured frames in each bar represent the record number for each group indicated in the legend.

Figure 2. Left: Histogram of the records of ITA08 (grey) and ITA10 (white), grouped according to earthquake magnitude. Right: Distance - magnitude scatter plot for ITA10 and ITA08: red circles are common data, green circles are data only included in the ITA08 dataset and grey circles are the new data included ITA10.

Figure 3. Left: Histogram of the records of ITA08 (grey) and ITA10 (white), grouped according to earthquake magnitude. Right: Distance - magnitude scatter plot for ITA10 and ITA08: red crosses are common data, black crosses are data used to derive ITA08 and blue crosses are the new data used to derive ITA10.

Figure 4. Histograms of records grouped according to site classes: ITA08 (left) and ITA10 (right).

Figure 5. Site classification for stations common to ITA10 and ITA08, according to the EC8 and SP schemes.

Figure 6. Unit covariance matrix for spectral acceleration at 0.1s (top) and 1s (bottom). The absolute value of each entry is shown. The negative entries are indicated with a black dot. Each column corresponds to a regression parameter (equations 1 to 3), in the following order: e_1, c_1, c_2, h, c_3, b_1, b_2, s_2, s_3, s_4, s_5, f_1, f_2, f_3, f_4.

Figure 7 Site coefficients obtained for the soil classes (left) and the different styles of faulting (right). Top: geometrical mean of the horizontal components (GeoH); bottom: vertical component (Z). On the left panels, letters from B through D indicate the EC8 site classes; on the right panel, R, SS, and N represent reverse, strike slip, and normal faulting, respectively

Figure 8. Comparisons between median predictions for PGA and PGV (black lines) ± 1 standard deviation (gray area) and observations (symbols) for the earthquakes indicated in the top of each plot. The comparison for M = 4.6 and unknown focal mechanism is performed considering data from 5 different earthquakes. Different symbols correspond to different site classes accordingly to Eurocode8 (CEN, 2003), as indicated below the plots.

Figure 9. Left: period-dependent total standard deviation (σ_{tot}) of the GMPE derived in this study (red circles). The within-event (black) and between-event (gray) components of

variability are shown as well. Right: comparison between σ_{tot} for this study (red circles) and ITA08 (blue triangles). The between-station components of variability for this study (gray) and ITA08 (green) are compared as well.

Figure 10 Within-event component of variability versus distance (left) and between-event distribution component of variability versus magnitude (right) obtained for PGA (top) and spectral accelerations at 0.1 and 1 s (middle and bottom, respectively).

Figure11. Comparison between ITA10 (red curve) and ITA08 (black curve) for an earthquake with M = 6.3. The observations refer to the records of L'Aquila mainshock. Left: SA (1s); right PGA.

Figure12. Comparison between ITA10 (red curve) and ITA08 (black curve) for an earthquake with M = 4.6.

Figure 13. Comparison between ITA10 (red curve) and ITA08 (black curve) for an earthquake with M = 6.3. The observations refer to the records of L'Aquila mainshock.

Tables

Table 1. Regression coefficients (see equations from 1 to 3) obtained for the geometrical mean of the horizontal components (GeoH). The columns sA through sE show the site coefficients for the EC8 classes. The columns f1 through f4 show the style of faulting coefficients for normal (f1), reverse (f2), strike slip (f3) and unknown (f4) mechanisms. The total (σ), the between-event (σ_B) and within-event (σ_W) standard deviations are shown as well.

T [s]	e1	c1	c2	h	c3	b1	b2	sA	sB	sC	sD	sE	f1	f2	f3	f4	σ_B	σ_W	σ
0.04	3.725	-1.976	0.422	9.445	2.70E-04	-3.15E-01	-7.87E-02	0	0.161	0.240	0.060	0.614	-4.42E-02	1.06E-01	-6.15E-02	0	0.154	0.307	0.343
0.07	3.906	-2.050	0.446	9.810	7.58E-04	-3.75E-01	-7.73E-02	0	0.154	0.235	0.057	0.536	-4.54E-02	1.03E-01	-5.76E-02	0	0.152	0.324	0.358
0.1	3.796	-1.794	0.415	9.500	2.55E-03	-2.90E-01	-6.51E-02	0	0.178	0.247	0.037	0.599	-6.56E-02	1.11E-01	-4.51E-02	0	0.154	0.328	0.363
0.15	3.799	-1.521	0.320	9.163	3.72E-03	-9.87E-02	-5.74E-02	0	0.174	0.240	0.148	0.740	-7.55E-02	1.23E-01	-4.77E-02	0	0.179	0.318	0.365
0.2	3.750	-1.379	0.280	8.502	3.84E-03	9.40E-03	-5.17E-02	0	0.156	0.234	0.115	0.556	-7.33E-02	1.06E-01	-3.28E-02	0	0.209	0.320	0.382
0.25	3.699	-1.340	0.254	7.912	3.26E-03	8.60E-02	-4.57E-02	0	0.182	0.245	0.154	0.414	-5.68E-02	1.10E-01	-5.34E-02	0	0.212	0.308	0.374
0.3	3.753	-1.414	0.255	8.215	2.19E-03	1.24E-01	-4.35E-02	0	0.201	0.244	0.213	0.301	-5.64E-02	8.77E-02	-3.13E-02	0	0.218	0.290	0.363
0.35	3.600	-1.320	0.253	7.507	2.32E-03	1.54E-01	-4.37E-02	0	0.220	0.257	0.243	0.235	-5.23E-02	9.05E-02	-3.82E-02	0	0.221	0.283	0.359
0.4	3.549	-1.262	0.233	6.760	2.19E-03	2.25E-01	-4.06E-02	0	0.229	0.255	0.226	0.202	-5.65E-02	9.27E-02	-3.63E-02	0	0.210	0.279	0.349
0.45	3.550	-1.261	0.223	6.775	1.76E-03	2.92E-01	-3.06E-02	0	0.226	0.271	0.237	0.181	-5.97E-02	8.86E-02	-2.89E-02	0	0.204	0.284	0.350
0.5	3.526	-1.181	0.184	5.992	1.86E-03	3.84E-01	-2.50E-02	0	0.218	0.280	0.263	0.168	-5.99E-02	8.50E-02	-2.52E-02	0	0.203	0.283	0.349
0.6	3.561	-1.230	0.178	6.382	1.14E-03	4.36E-01	-2.27E-02	0	0.219	0.296	0.355	0.142	-5.59E-02	7.90E-02	-2.31E-02	0	0.203	0.283	0.348
0.7	3.485	-1.172	0.154	5.574	9.42E-04	5.29E-01	-1.85E-02	0	0.210	0.303	0.496	0.134	-4.61E-02	8.96E-02	-4.35E-02	0	0.212	0.283	0.354
0.8	3.325	-1.115	0.163	4.998	9.09E-04	5.45E-01	-2.15E-02	0	0.210	0.304	0.621	0.150	-4.57E-02	7.95E-02	-3.38E-02	0	0.213	0.284	0.355
0.9	3.318	-1.137	0.154	5.231	4.83E-04	5.63E-01	-2.63E-02	0	0.212	0.315	0.680	0.154	-3.51E-02	7.15E-02	-3.64E-02	0	0.214	0.286	0.357
1	3.264	-1.114	0.140	5.002	2.54E-04	5.99E-01	-2.70E-02	0	0.221	0.332	0.707	0.152	-2.98E-02	6.60E-02	-3.62E-02	0	0.222	0.283	0.360
1.25	2.896	-0.986	0.173	4.340	7.83E-04	5.79E-01	-3.36E-02	0	0.244	0.365	0.717	0.183	-2.07E-02	6.14E-02	-4.07E-02	0	0.227	0.290	0.368
1.5	2.675	-0.960	0.192	4.117	8.02E-04	5.75E-01	-3.53E-02	0	0.251	0.375	0.667	0.203	-1.40E-02	5.05E-02	-3.65E-02	0	0.218	0.303	0.373
1.75	2.584	-1.006	0.205	4.505	4.27E-04	5.74E-01	-3.71E-02	0	0.252	0.357	0.593	0.220	1.54E-03	3.70E-02	-3.85E-02	0	0.219	0.305	0.376
2	2.537	-1.009	0.193	4.373	1.64E-04	5.97E-01	-3.67E-02	0	0.245	0.352	0.540	0.226	5.12E-03	3.50E-02	-4.01E-02	0	0.211	0.308	0.373

Table 2. Regression coefficients (see equations from 1 to 3) obtained for the vertical component (Z). The columns sA through sE show the site coefficients for the EC8 classes. The columns f1 through f4 show the style of faulting coefficients for normal (f1), reverse (f2), strike slip (f3) and unknown (f4) mechanisms. The total (σ), the between-event (σ_B) and within-event (σ_W) standard deviations are shown as well.

T [s]	e1	c1	c2	h	c3	b1	b2	sA	sB	sC	sD	sE	f1	f2	f3	f4	σ_B	σ_W	σ
0.04	3.823	-1.892	0.301	7.754	7.85E-04	1.38E-02	-2.99E-02	0	0.179	0.228	0.133	0.428	-5.88E-02	7.27E-02	-1.39E-02	0	0.140	0.299	0.330
0.07	3.936	-1.818	0.305	8.385	2.29E-03	-2.60E-03	-2.67E-02	0	0.168	0.231	0.162	0.318	-9.70E-02	9.50E-02	2.03E-03	0	0.152	0.304	0.340
0.1	3.801	-1.579	0.275	8.946	3.68E-03	4.34E-02	-2.60E-02	0	0.190	0.181	0.178	0.342	-9.09E-02	8.36E-02	7.30E-03	0	0.157	0.296	0.335
0.15	3.684	-1.348	0.210	8.742	4.39E-03	1.54E-01	-3.05E-02	0	0.204	0.191	0.288	0.407	-7.52E-02	9.17E-02	-1.65E-02	0	0.177	0.284	0.335
0.2	3.703	-1.493	0.258	10.140	3.18E-03	5.99E-02	-4.45E-02	0	0.205	0.191	0.278	0.319	-7.93E-02	9.97E-02	-2.05E-02	0	0.182	0.277	0.332
0.25	3.624	-1.439	0.248	9.825	2.77E-03	1.26E-01	-3.54E-02	0	0.193	0.172	0.344	0.245	-7.35E-02	9.65E-02	-2.30E-02	0	0.193	0.269	0.331
0.3	3.519	-1.352	0.239	8.936	2.74E-03	1.87E-01	-3.31E-02	0	0.170	0.179	0.356	0.163	-7.86E-02	7.02E-02	8.41E-03	0	0.198	0.265	0.331
0.35	3.317	-1.185	0.211	7.700	3.18E-03	2.34E-01	-3.53E-02	0	0.157	0.191	0.372	0.167	-7.90E-02	7.76E-02	1.41E-03	0	0.194	0.258	0.323
0.4	3.161	-1.199	0.264	7.697	2.88E-03	1.65E-01	-4.28E-02	0	0.149	0.182	0.457	0.132	-7.57E-02	9.12E-02	-1.55E-02	0	0.205	0.262	0.333
0.45	3.280	-1.287	0.246	8.131	1.78E-03	2.12E-01	-4.26E-02	0	0.147	0.200	0.459	0.105	-7.78E-02	8.31E-02	-5.32E-03	0	0.217	0.266	0.343
0.5	3.358	-1.311	0.221	8.182	1.24E-03	2.93E-01	-3.31E-02	0	0.148	0.194	0.486	0.098	-6.91E-02	8.29E-02	-1.38E-02	0	0.214	0.262	0.338
0.6	3.347	-1.302	0.223	8.409	1.08E-03	3.80E-01	-1.65E-02	0	0.150	0.197	0.512	0.082	-5.75E-02	8.08E-02	-2.34E-02	0	0.230	0.259	0.347
0.7	3.072	-1.168	0.222	6.960	1.18E-03	3.95E-01	-2.58E-02	0	0.157	0.213	0.518	0.099	-3.73E-02	8.56E-02	-4.83E-02	0	0.239	0.270	0.361
0.8	2.941	-1.124	0.222	6.679	1.14E-03	4.14E-01	-3.01E-02	0	0.170	0.219	0.513	0.108	-2.51E-02	6.94E-02	-4.44E-02	0	0.241	0.271	0.363
0.9	2.795	-1.031	0.218	5.763	1.51E-03	4.30E-01	-3.48E-02	0	0.182	0.217	0.494	0.096	-1.72E-02	6.90E-02	-5.18E-02	0	0.248	0.269	0.366
1	2.709	-0.952	0.202	4.806	1.63E-03	5.07E-01	-2.44E-02	0	0.177	0.229	0.456	0.092	-1.06E-02	6.80E-02	-5.73E-02	0	0.248	0.269	0.365
1.25	2.536	-0.854	0.194	4.433	1.91E-03	6.04E-01	-1.30E-02	0	0.179	0.253	0.407	0.115	-4.80E-03	6.95E-02	-6.47E-02	0	0.245	0.277	0.370
1.5	2.523	-0.808	0.147	4.439	2.18E-03	7.43E-01	-2.08E-03	0	0.148	0.262	0.392	0.130	5.87E-03	5.30E-02	-5.89E-02	0	0.247	0.291	0.382
1.75	2.292	-0.684	0.142	2.995	2.63E-03	7.95E-01	7.00E-03	0	0.134	0.259	0.346	0.117	1.26E-03	4.98E-02	-5.11E-02	0	0.243	0.298	0.384
2	2.126	-0.645	0.150	2.219	2.83E-03	7.54E-01	-4.88E-03	0	0.148	0.256	0.297	0.117	4.10E-03	4.90E-02	-5.31E-02	0	0.237	0.302	0.384

Table 3. Standard deviations of the regression coefficients obtained for the geometrical mean of the horizontal components (GeoH).

T [s]	e1	c1	c2	h	c3	b1	b2	sA	sB	sC	sD	sE	f1	f2	f3	f4
0.04	0.296	0.215	0.0739	1.659	1.28E-03	0.169	0.0253	0	0.0275	0.0331	0.0503	0.0573	2.48E-02	3.65E-02	3.73E-02	0
0.07	0.349	0.294	0.0822	1.675	1.77E-03	0.180	0.0305	0	0.0283	0.0282	0.0439	0.0429	2.47E-02	3.18E-02	3.73E-02	0
0.1	0.365	0.316	0.0890	2.018	1.88E-03	0.170	0.0284	0	0.0326	0.0357	0.0462	0.0503	2.47E-02	3.51E-02	3.67E-02	0
0.15	0.344	0.313	0.0788	2.249	1.99E-03	0.177	0.0318	0	0.0326	0.0284	0.0441	0.0517	2.08E-02	3.21E-02	3.13E-02	0
0.2	0.298	0.267	0.0729	2.211	1.74E-03	0.164	0.0257	0	0.0295	0.0263	0.0385	0.0624	2.16E-02	3.04E-02	3.29E-02	0
0.25	0.394	0.299	0.0599	2.669	1.88E-03	0.143	0.0278	0	0.0267	0.0320	0.0524	0.0702	2.29E-02	3.41E-02	3.36E-02	0
0.3	0.367	0.248	0.0434	2.023	1.62E-03	0.108	0.0243	0	0.0312	0.0349	0.0510	0.0777	2.02E-02	2.89E-02	3.42E-02	0
0.35	0.288	0.213	0.0498	1.944	1.38E-03	0.130	0.0262	0	0.0280	0.0375	0.0611	0.0566	1.82E-02	2.86E-02	3.47E-02	0
0.4	0.302	0.231	0.0566	1.909	1.41E-03	0.129	0.0236	0	0.0290	0.0369	0.0498	0.0650	2.03E-02	3.61E-02	3.71E-02	0
0.45	0.266	0.192	0.0448	1.747	1.33E-03	0.120	0.0235	0	0.0264	0.0323	0.0518	0.0549	1.73E-02	2.70E-02	3.13E-02	0
0.5	0.342	0.229	0.0492	1.835	1.54E-03	0.142	0.0310	0	0.0329	0.0328	0.0598	0.0615	1.65E-02	3.23E-02	3.34E-02	0
0.6	0.293	0.182	0.0462	1.740	1.14E-03	0.124	0.0254	0	0.0255	0.0321	0.0509	0.0646	1.98E-02	2.67E-02	3.33E-02	0
0.7	0.234	0.166	0.0384	1.430	1.10E-03	0.113	0.0282	0	0.0312	0.0370	0.0769	0.0702	2.26E-02	2.65E-02	3.00E-02	0
0.8	0.274	0.170	0.0556	1.626	1.17E-03	0.125	0.0252	0	0.0304	0.0365	0.0773	0.0585	2.09E-02	3.34E-02	3.40E-02	0
0.9	0.262	0.174	0.0419	1.671	1.26E-03	0.106	0.0234	0	0.0276	0.0427	0.0622	0.0671	2.30E-02	3.00E-02	3.63E-02	0
1	0.232	0.141	0.0440	1.427	8.63E-04	0.111	0.0251	0	0.0267	0.0415	0.0622	0.0608	2.60E-02	2.84E-02	3.78E-02	0
1.25	0.208	0.125	0.0436	1.175	9.44E-04	0.099	0.0212	0	0.0312	0.0310	0.0542	0.0601	2.42E-02	3.29E-02	3.81E-02	0
1.5	0.251	0.180	0.0461	1.606	1.29E-03	0.113	0.0265	0	0.0268	0.0422	0.0632	0.0536	1.90E-02	3.31E-02	3.38E-02	0
1.75	0.238	0.166	0.0491	1.595	1.14E-03	0.113	0.0250	0	0.0286	0.0374	0.0652	0.0682	2.61E-02	3.38E-02	4.25E-02	0
2	0.259	0.144	0.0545	1.287	1.09E-03	0.135	0.0282	0	0.0345	0.0369	0.0787	0.0810	2.32E-02	3.09E-02	3.87E-02	0

Table 4. Standard deviations of the regression coefficients obtained for the vertical component (*Z*).

T [s]	e1	c1	c2	h	c3	b1	b2	sA	sB	sC	sD	sE	f1	f2	f3	f4
0.04	0.306	0.200	0.0695	1.583	1.22E-03	0.161	0.0255	0	0.0236	0.0284	0.0619	0.0576	2.49E-02	3.74E-02	3.91E-02	0
0.07	0.361	0.298	0.0810	1.912	1.78E-03	0.173	0.0282	0	0.0275	0.0265	0.0607	0.0363	2.49E-02	2.84E-02	3.68E-02	0
0.1	0.334	0.270	0.0784	2.197	1.56E-03	0.158	0.0294	0	0.0358	0.0317	0.0448	0.0547	2.15E-02	3.06E-02	3.14E-02	0
0.15	0.291	0.233	0.0656	1.964	1.42E-03	0.135	0.0244	0	0.0302	0.0249	0.0592	0.0466	1.60E-02	2.26E-02	2.43E-02	0
0.2	0.301	0.244	0.0735	1.917	1.52E-03	0.163	0.0255	0	0.0257	0.0259	0.0495	0.0613	1.83E-02	2.76E-02	2.77E-02	0
0.25	0.427	0.335	0.0615	2.983	1.97E-03	0.136	0.0264	0	0.0264	0.0271	0.0565	0.0616	1.94E-02	3.38E-02	3.58E-02	0
0.3	0.352	0.255	0.0518	2.125	1.54E-03	0.121	0.0243	0	0.0339	0.0274	0.0530	0.0693	2.24E-02	2.60E-02	3.21E-02	0
0.35	0.319	0.250	0.0496	2.459	1.58E-03	0.116	0.0223	0	0.0232	0.0309	0.0628	0.0521	2.21E-02	2.61E-02	3.48E-02	0
0.4	0.311	0.264	0.0637	2.305	1.54E-03	0.136	0.0226	0	0.0251	0.0313	0.0599	0.0660	2.13E-02	3.01E-02	3.17E-02	0
0.45	0.339	0.258	0.0477	2.375	1.77E-03	0.125	0.0244	0	0.0231	0.0288	0.0577	0.0603	1.91E-02	3.03E-02	3.77E-02	0
0.5	0.315	0.232	0.0547	1.978	1.49E-03	0.153	0.0310	0	0.0256	0.0315	0.0669	0.0644	1.94E-02	3.02E-02	3.63E-02	0
0.6	0.324	0.231	0.0559	2.130	1.38E-03	0.132	0.0240	0	0.0322	0.0305	0.0518	0.0535	2.09E-02	3.02E-02	3.96E-02	0
0.7	0.278	0.220	0.0516	2.120	1.36E-03	0.129	0.0285	0	0.0299	0.0301	0.0849	0.0579	2.34E-02	2.85E-02	3.38E-02	0
0.8	0.348	0.256	0.0566	2.776	1.59E-03	0.126	0.0275	0	0.0330	0.0329	0.0783	0.0614	2.07E-02	3.54E-02	3.34E-02	0
0.9	0.308	0.240	0.0505	2.555	1.52E-03	0.119	0.0269	0	0.0285	0.0373	0.0635	0.0626	2.50E-02	3.10E-02	3.91E-02	0
1	0.269	0.182	0.0529	2.204	1.10E-03	0.138	0.0291	0	0.0308	0.0389	0.0715	0.0588	2.70E-02	3.31E-02	4.51E-02	0
1.25	0.272	0.177	0.0455	1.950	1.23E-03	0.120	0.0261	0	0.0340	0.0310	0.0616	0.0640	2.62E-02	3.34E-02	3.70E-02	0
1.5	0.350	0.248	0.0541	2.584	1.74E-03	0.134	0.0292	0	0.0252	0.0371	0.0683	0.0574	2.22E-02	4.04E-02	3.88E-02	0
1.75	0.302	0.206	0.0495	2.468	1.43E-03	0.124	0.0268	0	0.0301	0.0369	0.0546	0.0749	2.81E-02	3.77E-02	4.61E-02	0
2	0.243	0.132	0.0551	1.582	1.09E-03	0.130	0.0272	0	0.0350	0.0339	0.0846	0.0746	3.04E-02	3.74E-02	4.78E-02	0

Table 5. Regression coefficients for peak ground acceleration (PGA) and velocity (PGV), considering the geometrical mean of the horizontal components (GeoH) and the vertical component (Z).

	PGA_GeoH	PGV_GeoH	PGA_Z	PGV_Z
e1	3.672	2.305	3.511	2.099
c1	-1.940	-1.517	-1.741	-1.552
c2	0.413	0.328	0.324	0.371
h	10.322	7.879	9.052	9.629
c3	1.34E-04	0	1.28E-03	0
b1	-0.262	0.236	9.04E-03	0.228
b2	-0.0707	-6.86E-03	-0.0270	7.56E-03
sA	0	0	0	0
sB	0.162	0.205	0.167	0.156
sC	0.240	0.289	0.204	0.211
sD	0.105	0.321	0.190	0.316
sE	0.570	0.428	0.350	0.233
f1	-5.03E-02	-3.08E-02	-7.09E-02	-4.40E-02
f2	1.05E-01	7.54E-02	7.79E-02	8.49E-02
f3	-5.44E-02	-4.46E-02	-6.96E-03	-4.09E-02
f4	0	0	0	0
σ_B	0.172	0.194	0.160	0.190
σ_W	0.290	0.270	0.270	0.242
σ	0.337	0.332	0.314	0.308

Table 6 Standard deviation of the regression coefficients for peak ground acceleration (PGA) and velocity (PGV), considering the geometrical mean of the horizontal components (GeoH) and the vertical component (Z).

	PGA_GeoH	PGV_GeoH	PGA_Z	PGV_Z
e1	3.16E-01	1.62E-01	3.01E-01	1.49E-01
c1	2.58E-01	5.69E-02	2.61E-01	6.03E-02
c2	6.85E-02	4.61E-02	6.76E-02	5.28E-02
h	1.61E+00	9.43E-01	1.84E+00	1.03E+00
c3	1.57E-03	0	1.62E-03	1.16E-01
b1	1.55E-01	1.11E-01	1.66E-01	2.32E-02
b2	2.76E-02	2.38E-02	2.96E-02	7.56E-03
sA	0	0	0	0
sB	2.89E-02	2.81E-02	3.05E-02	2.56E-02
sC	3.22E-02	3.40E-02	2.90E-02	3.07E-02
sD	5.22E-02	5.49E-02	5.56E-02	6.80E-02
sE	4.49E-02	4.61E-02	4.18E-02	4.20E-02
f1	2.11E-02	1.80E-02	1.97E-02	1.64E-02
f2	2.96E-02	3.09E-02	2.77E-02	2.84E-02
f3	3.55E-02	3.33E-02	3.43E-02	3.36E-02
f4	0	0	0	0

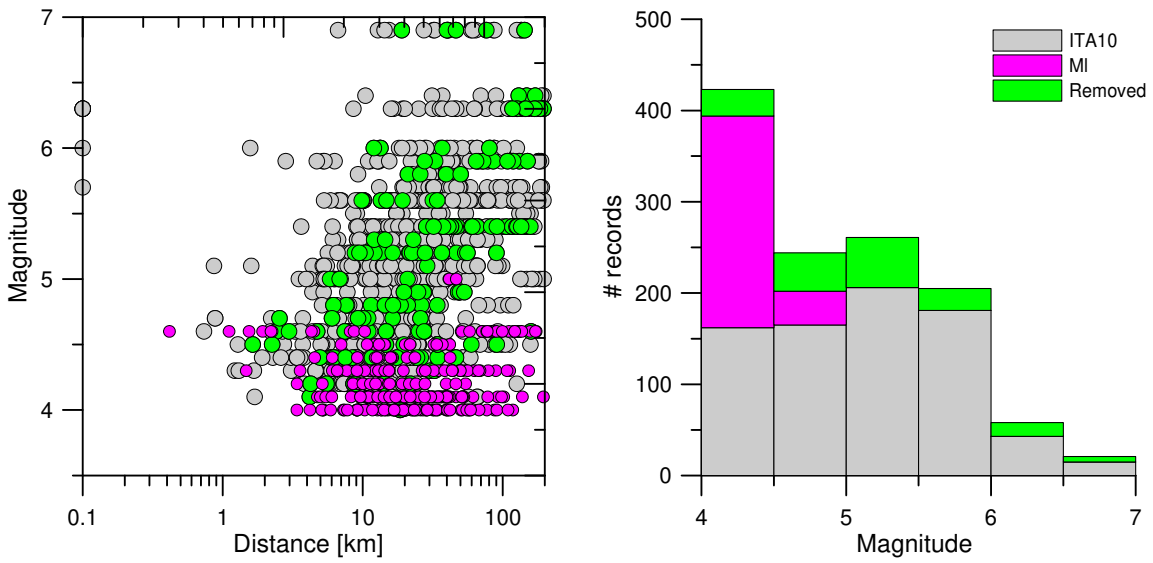
Magnitude
Distance [km]
0.1
1
10
100
4
5
6
7
records
Magnitude
0
100
200
300
400
500
ITA10
MI
Removed

Figure 1

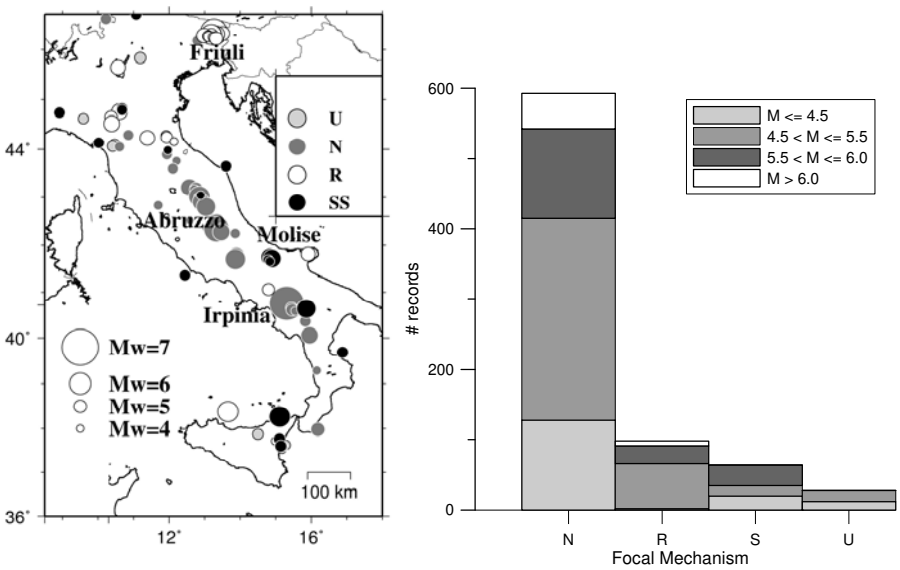
Friuli
Abruzzo
Molise
Irpinia
U
N
R
SS
Mw=7
Mw=6
Mw=5
Mw=4
100 km
44°
40°
36°
12°
16°
600
400
200
0
records
M <= 4.5
4.5 < M <= 5.5
5.5 < M <= 6.0
M > 6.0
N
R
S
U
Focal Mechanism

Figure 2.

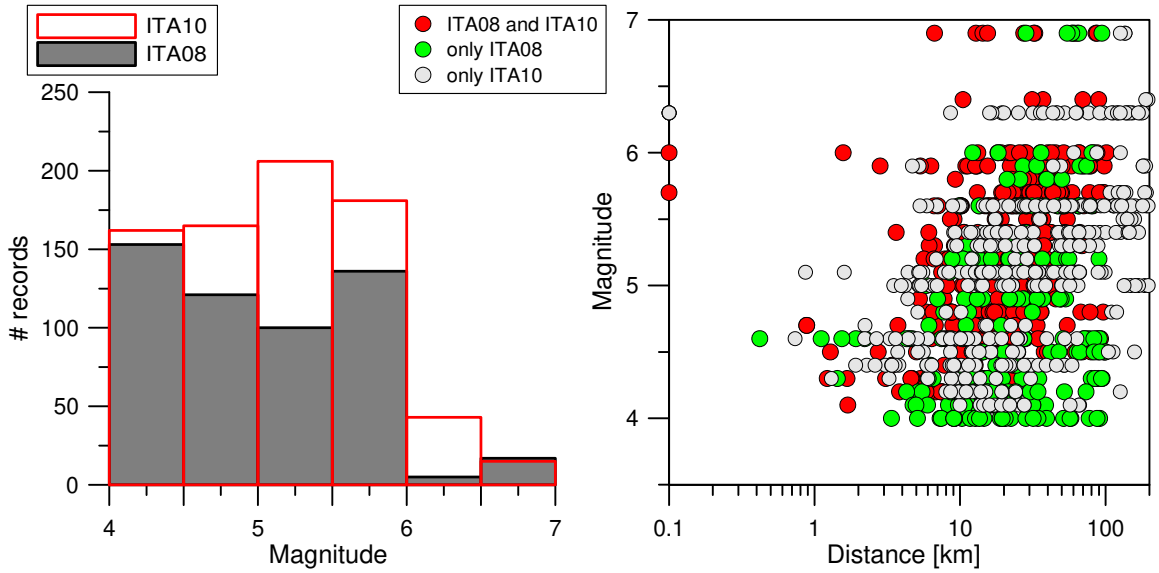
ITA10
ITA08
ITA08 and ITA10
only ITA08
only ITA10
records
Magnitude
Magnitude
Distance [km]

Figure 3.

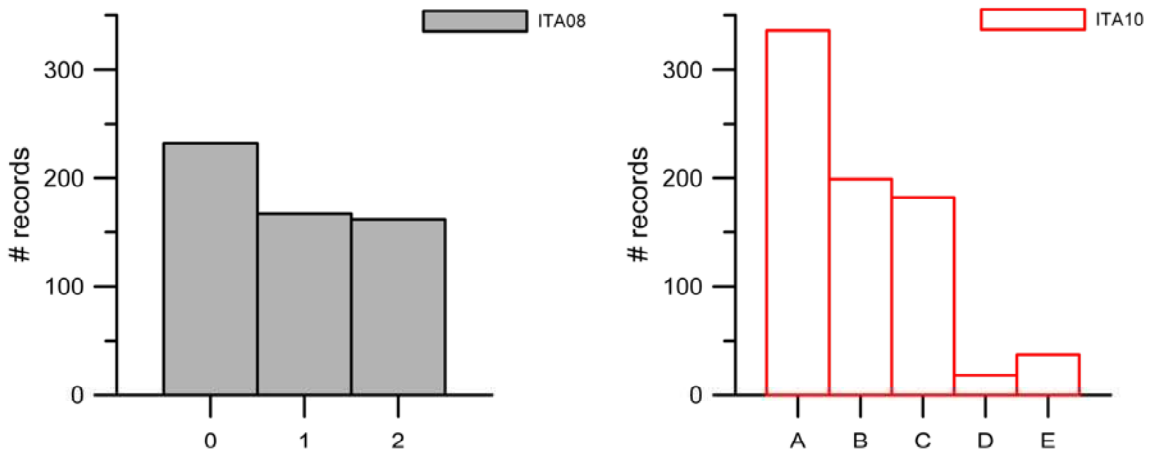

Figure 4. Histograms of records grouped according to site classes: ITA08 (left) and ITA10 (right).

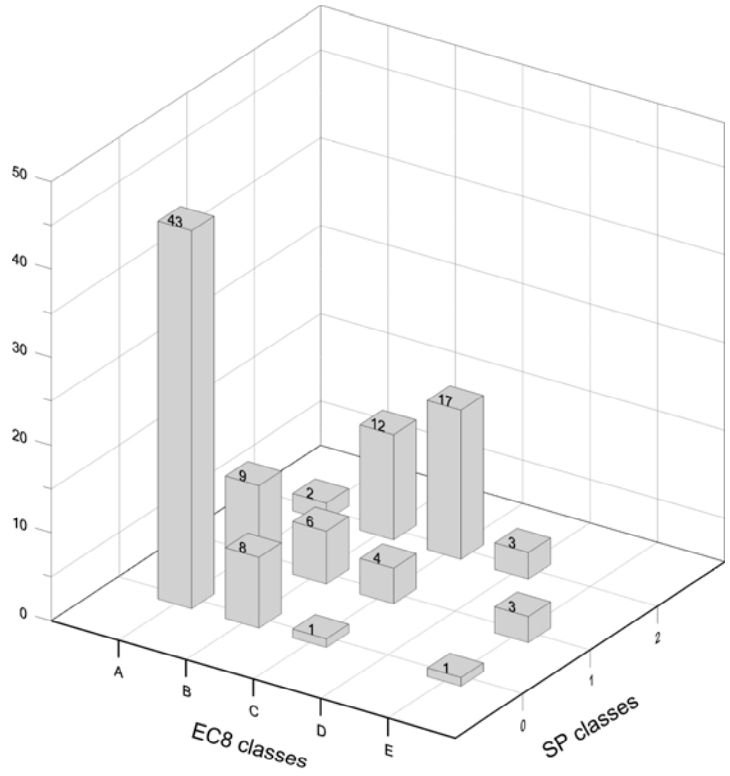

Figure 5. Site classification for stations common to ITA10 and ITA08, according to the EC8 and SP schemes.

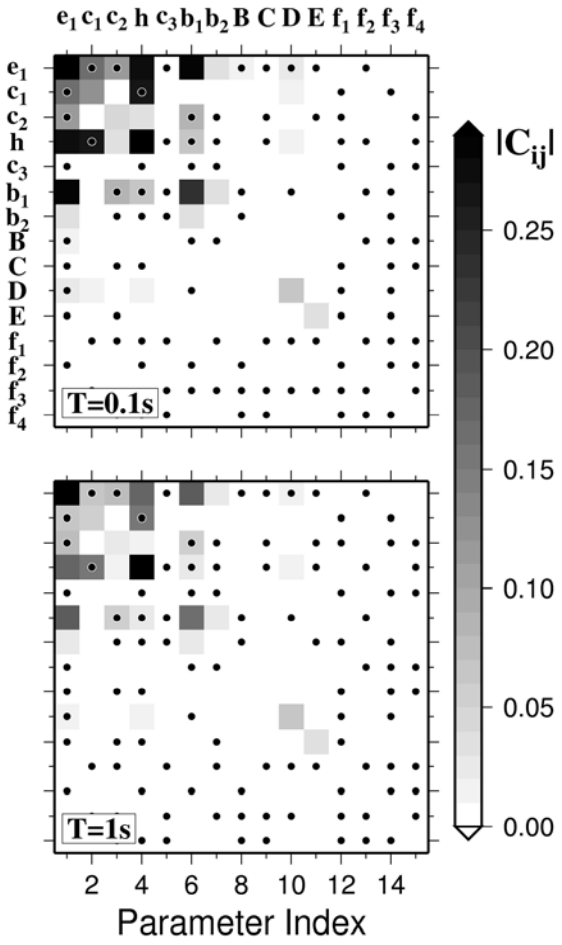
e1 c1 c2 h c3 b1 b2 B C D E f1 f2 f3 f4
e1
c1
c2
h
c3
b1
b2
B
C
D
E
f1
f2
f3
f4
T=0.1s
T=1s
|Cij|
0.25
0.20
0.15
0.10
0.05
0.00
2 4 6 8 10 12 14
Parameter Index

Figure 6.

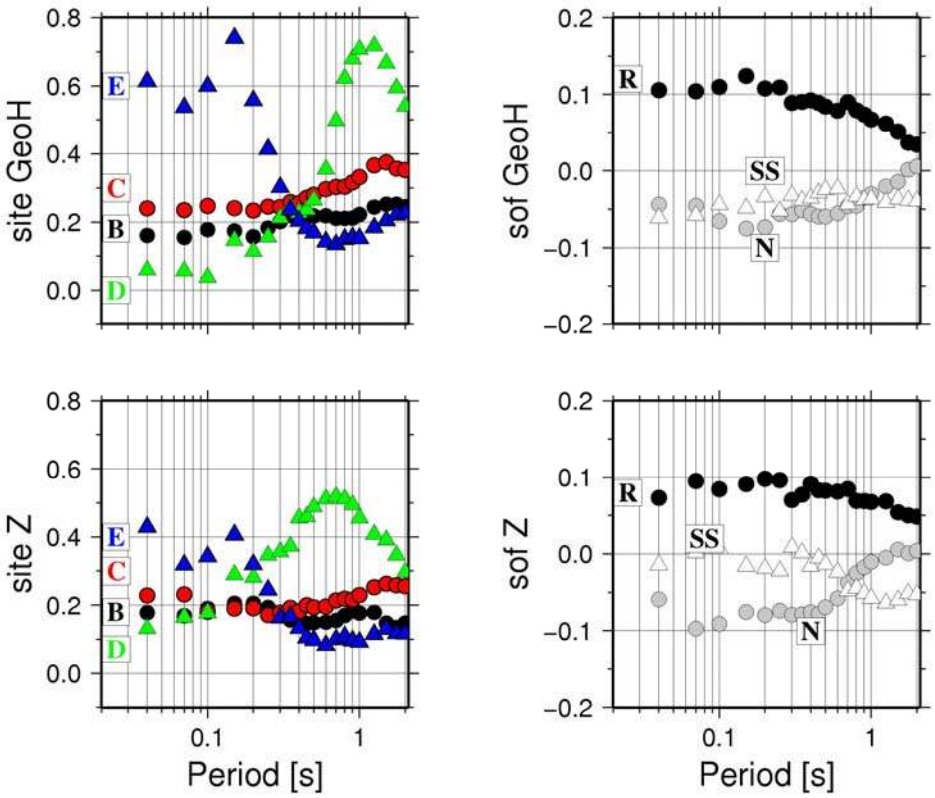
site GeoH
sof GeoH
site Z
sof Z
E
C
B
D
R
SS
N
Period [s]
0.8
0.6
0.4
0.2
0.0
0.1
−0.1
−0.2
1

Figure 7

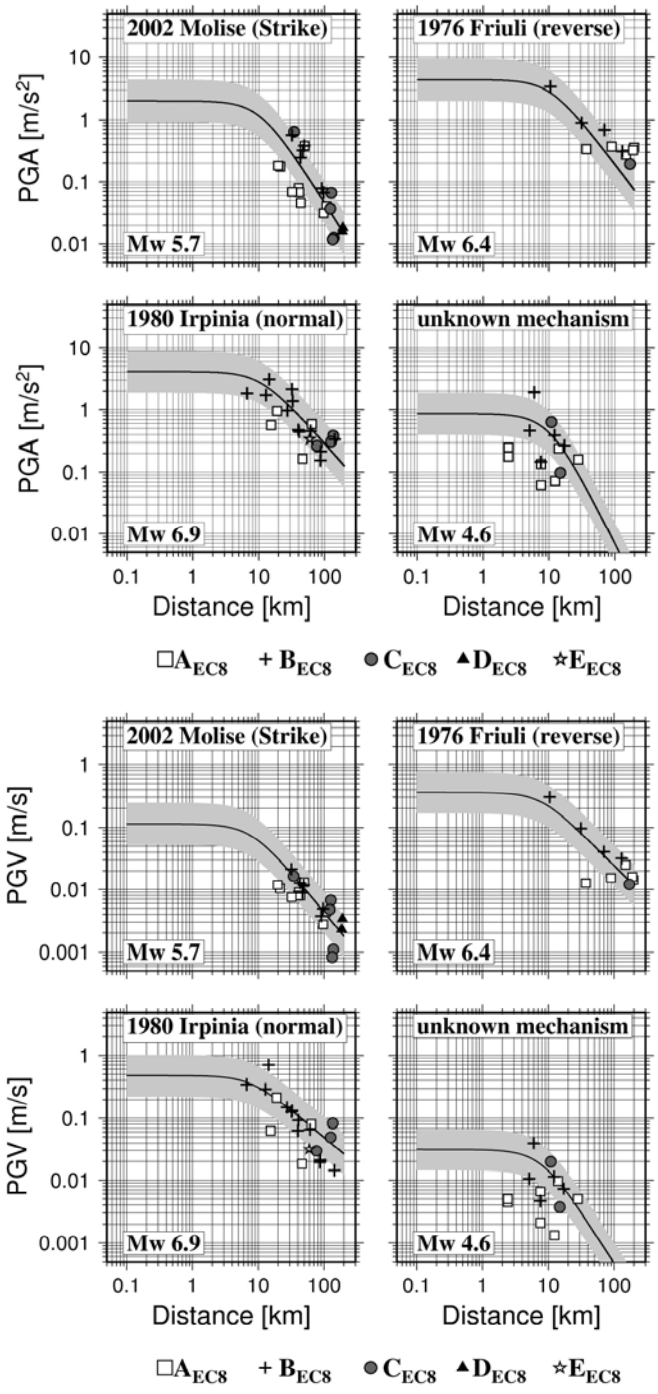
2002 Molise (Strike)
1976 Friuli (reverse)
1980 Irpinia (normal)
unknown mechanism
Mw 5.7
Mw 6.4
Mw 6.9
Mw 4.6
PGA [m/s²]
PGV [m/s]
Distance [km]
A_EC8 B_EC8 C_EC8 D_EC8 E_EC8

Figure 8..

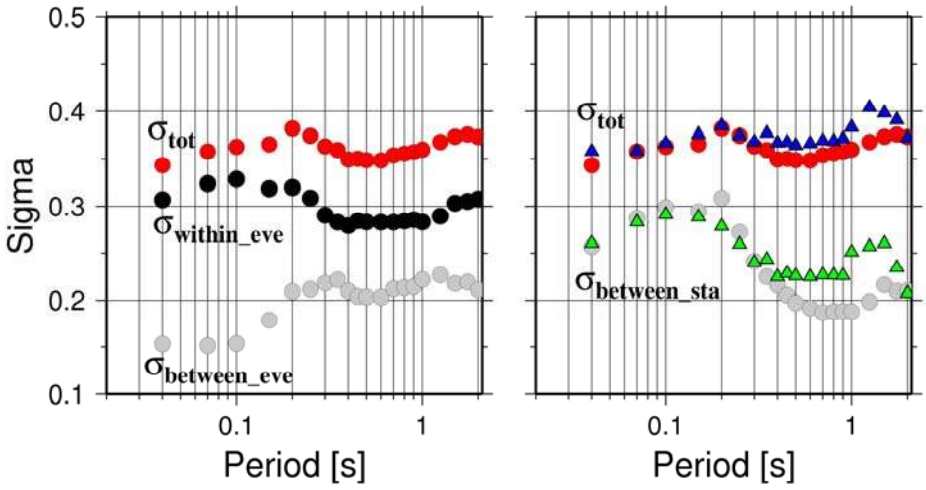
0.5
0.4
0.3
0.2
0.1
Sigma
σtot
σwithin_eve
σbetween_eve
0.1
1
Period [s]
σtot
σbetween_sta
0.1
1
Period [s]

Figure 9.

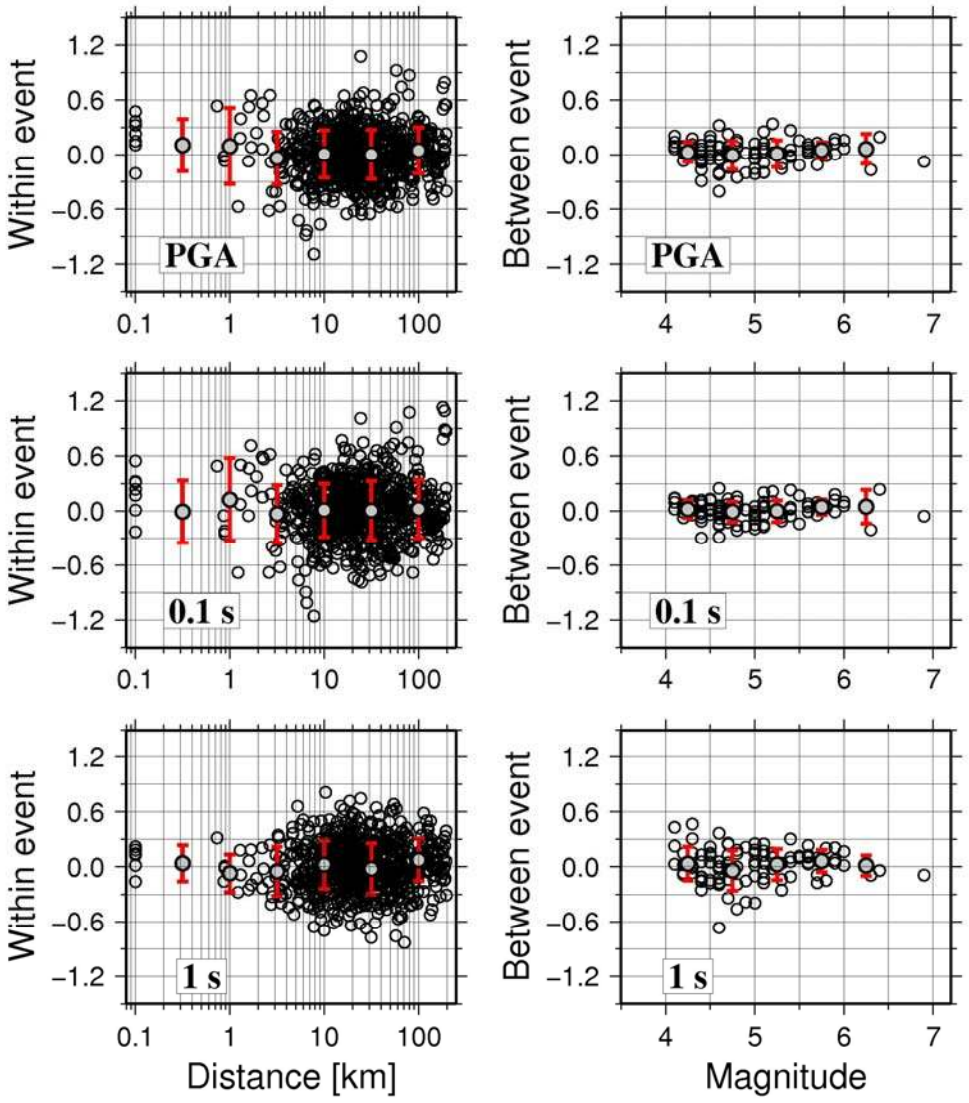
Within event
Between event
PGA
0.1 s
1 s
1.2
0.6
0.0
−0.6
−1.2
0.1
1
10
100
4
5
6
7
Distance [km]
Magnitude

Figure 10

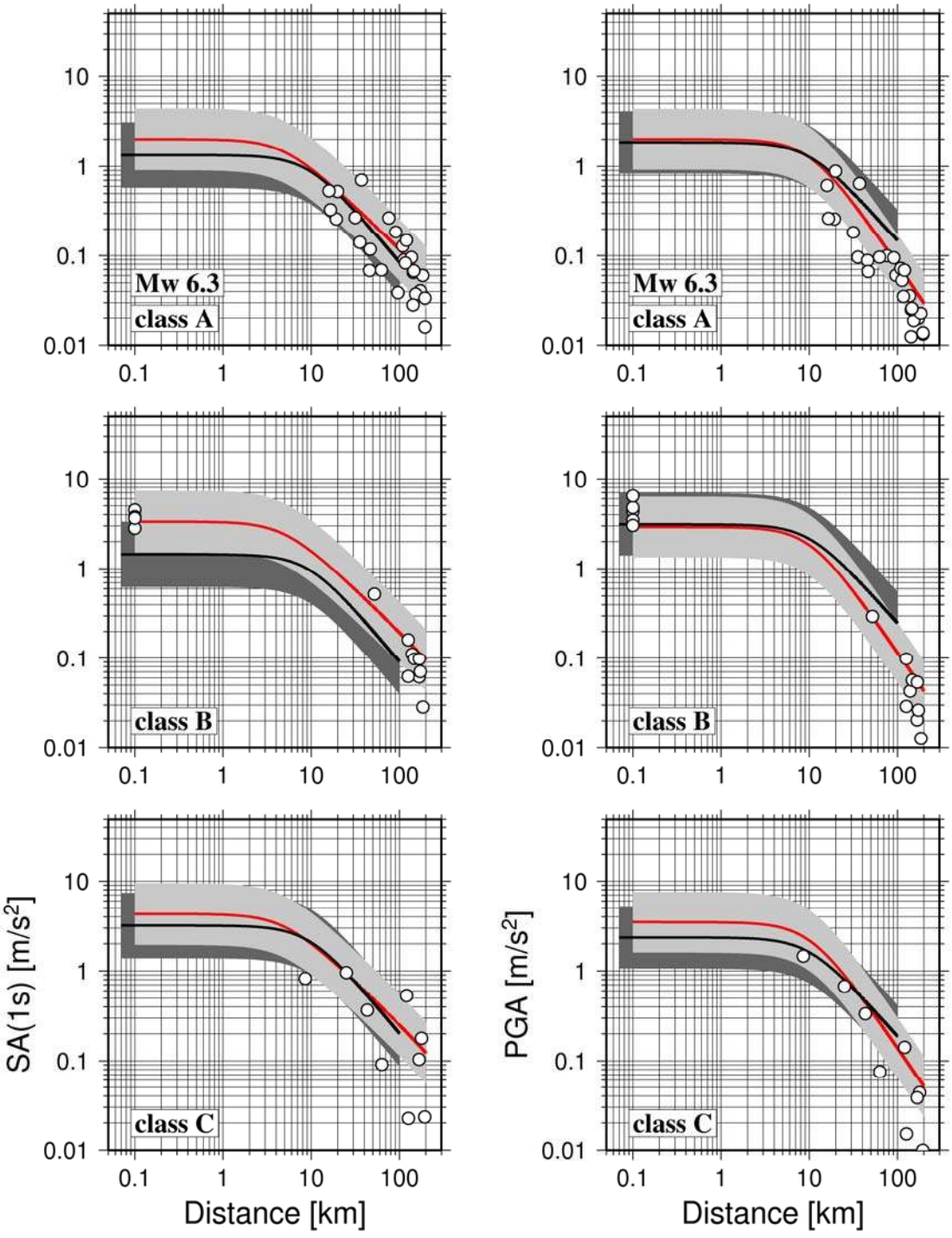
Mw 6.3
class A
Mw 6.3
class A
class B
class B
class C
class C
SA(1s) [m/s²]
PGA [m/s²]
Distance [km]
Distance [km]
0.01
0.1
1
10
100

Figure11.

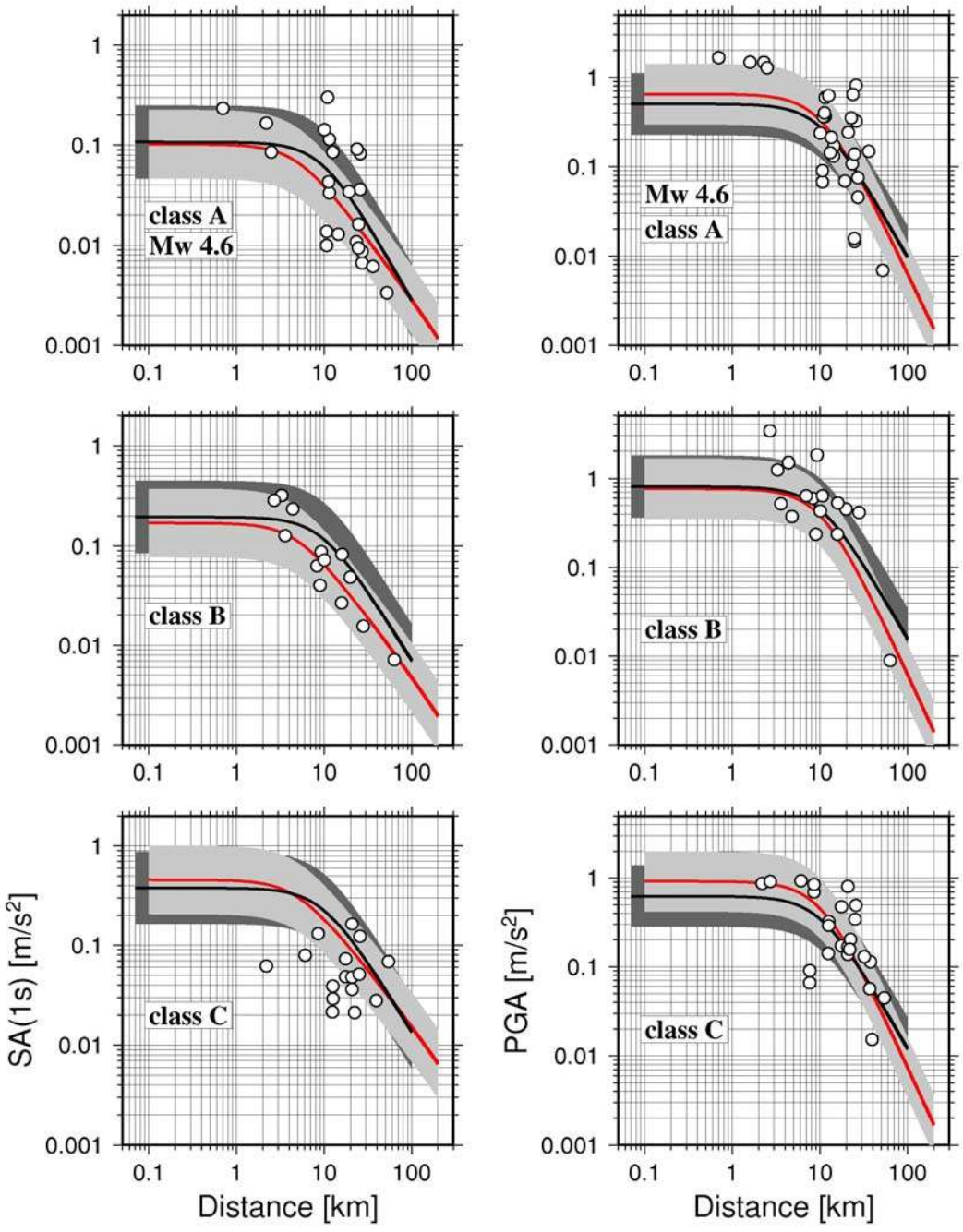
class A
Mw 4.6
Mw 4.6
class A
class B
class B
class C
class C
SA(1s) [m/s²]
PGA [m/s²]
Distance [km]
Distance [km]
1
0.1
0.01
0.001
0.1
1
10
100

Figure12.

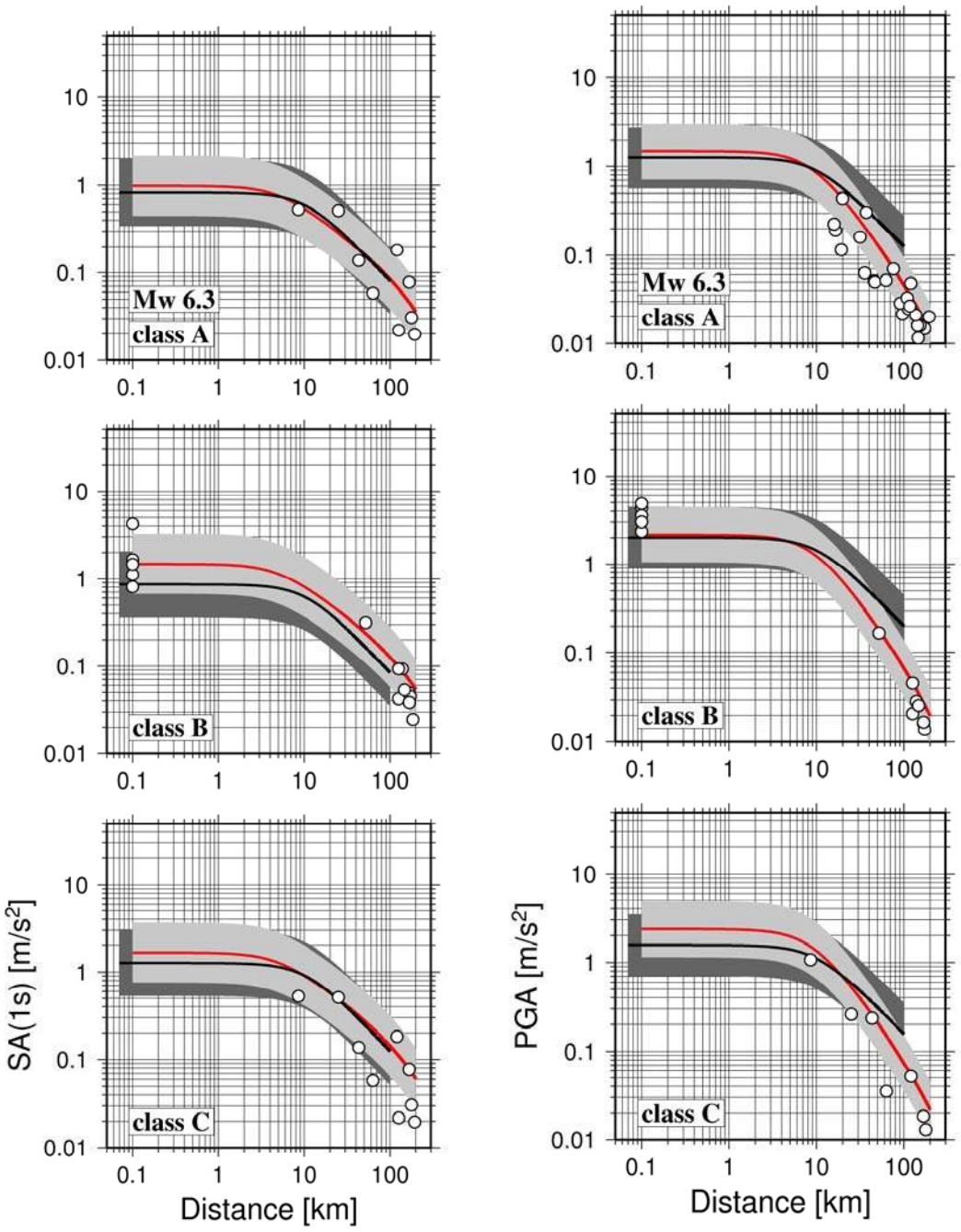
Mw 6.3
class A
class B
class C
SA(1s) [m/s²]
PGA [m/s²]
Distance [km]
0.01
0.1
1
10
100

Figure 13.